CHEMISTRY OF MATERIALS
Article

Chem. Mater. **2009,** *21,* 4203–4209 4203
DOI:10.1021/cm9007238

X-ray Absorption near Edge Structure and Crystallographic Studies of the Mixed Valence Oxides $CaRu_{1-x}Mn_xO_3$

Qingdi Zhou,[†] Brendan J. Kennedy,*[,†] Zhaoming Zhang,[‡] Ling-Yun Jang,[§] and Jade B. Aitken[†]

[†]*School of Chemistry, The University of Sydney, Sydney, New South Wales, 2006, Australia,* [‡]*Institute of Materials Engineering, Australian Nuclear Science and Technology Organisation, Private Mail Bag 1, Menai, New South Wales, 2234, Australia, and* [§]*Research Division, National Synchrotron Radiation Research Center, Hsinchu 300, Taiwan*

Received March 13, 2009. Revised Manuscript Received July 9, 2009

Eleven members of the series $CaRu_{1-x}Mn_xO_3$ with $0 \le x \le 1$ have been prepared and characterized using a combination of Mn K-edge and Ru $L_{3,2}$-edge X-ray absorption near edge structure spectroscopy and high resolution synchrotron X-ray powder diffraction. A complex distribution of four $Mn^{3+/4+}$ and $Ru^{4+/5+}$ oxidation states was observed and quantified. When incorporated into $CaRuO_3$ at low doping levels, the Mn is present as Mn^{3+} and Mn^{4+}, with the nominal Mn oxidation state increasing with x (from 3.6 at $x = 0.1$ to 4 at $x = 1$). The Ru exists predominantly as Ru^{5+} in $CaMnO_3$ with the nominal Ru valency as 4.8 at $x = 0.9$. The formation of $Mn^{3+/4+}-Ru^{4+/5+}$ redox pairs accounts for the unusual chemical composition dependence of the cell volume, evident from the diffraction studies. The coexistence of mixed valence redox pairs is also believed to contribute to the phase separation observed at $0.1 \le x \le 0.6$.

Introduction

The itinerant ferromagnetism observed in $SrRuO_3$ is one of the many intriguing examples of unexpected physical properties exhibited by perovskite-type ruthenium oxides, another example of which is the superconductivity in Sr_2RuO_4.[1] $SrRuO_3$ is a highly correlated, narrow-band metallic ferromagnet with a Curie temperature $T_c \sim 160$ K,[2,3] whereas the isostructural Ca compound $CaRuO_3$ does not exhibit any magnetic ordering.[4] Cao et al.[5] reported that doping of $CaRuO_3$ with a small amount of Sn results in a transformation to a magnetically ordered phase. Subsequently, He and Cava[6] independently showed that partially replacing the Ru, in $CaRuO_3$, with various magnetic and nonmagnetic ions induces ferromagnetism in the resulting $CaRu_{1-x}M_xO_3$ ternary oxides. He and Cava[6,7] referred to this phenomenon as "disorder-induced ferromagnetism" and considered it to be a phenomenon that is specific to $CaRuO_3$.[7] Raveau et al.[8] also noted unusual magnetic behavior in Ru doped $CaMnO_3$. Of the various systems studied by He and Cava, the Mn doped system is most notable because of the large magnetic moment and high T_c displayed by members of the series $CaRu_{1-x}Mn_xO_3$.[6] The ferromagnetism exhibited in this series is more remarkable given that neither end member shows any ferromagnetism.

In another study of the $CaMn_{1-x}Ru_xO_3$ oxides, Maignan and co-workers[9] described the ferromagnetism in terms of the double exchange interaction between Mn^{4+} and Mn^{3+} ions. The presence of Mn^{3+} was explained by assuming that, upon doping $CaMnO_3$ with Ru, the Mn^{4+} cations were replaced by Mn^{3+} and Ru^{5+} and the oxides with $0 < x \le 0.5$ were formally $CaMn_{1-2x}^{4+}Mn_x^{3+}Ru_x^{5+}O_3$. No quantitative explanation for the Mn-composition dependence of the ferromagnetism was given because the system was considered to be highly inhomogeneous.

The presence of mixed-valence states of the Mn and Ru ions is consistent with the unusual composition dependence of the lattice constants and the unit cell volume observed in the $CaRu_{1-x}Mn_xO_3$ series.[10] Direct evidence for the coexistence of the various valence states is, however, limited. Taniguchi and co-workers[10] reported Mn 2p and Ru 3p X-ray photoelectron spectra, suggestive of the presence of the $Ru^{5+}-Mn^{3+}$ pairs. However, no quantitative results could be directly obtained from X-ray photoelectron spectroscopy (XPS) due to the limitations of this technique. A better technique to use would be X-ray

*Corresponding author. E-mail: b.kennedy@chem.usyd.edu.au.

(1) Maeno, Y.; Hashimoto, H.; Yoshida, K.; Nishizaki, S.; Fujita, T.; Bednorz, J. G.; Lichtenberg, F. *Nature* **1994**, *372*, 532.
(2) Bouchard, R. J.; Gillson, J. L. *Mater. Res. Bull.* **1972**, *7*, 873.
(3) Longo, J. M.; Raccah, P. M.; Goodenough, J. B. *J. Appl. Phys.* **1968**, *39*, 1327.
(4) Felner, I.; Nowik, I.; Bradaric, I.; Gospodinov, M. *Phys. Rev. B* **2000**, *62*, 11332.
(5) Cao, G.; McCall, S.; Bolivar, J.; Shepard, M.; Freibert, F.; Henning, P.; Crow, J. E.; Yuen, T. *Phys. Rev. B* **1996**, *54*, 15144.
(6) He, T.; Cava, R. J. *J. Phys.: Condens. Matter* **2001**, *13*, 8347.
(7) He, T.; Cava, R. J. *Phys. Rev. B* **2001**, *63*, 172403.
(8) Raveau, B.; Maignan, A.; Martin, C.; Hervieu, M. *J. Supercond.* **2001**, *14*, 217.
(9) Maignan, A.; Martin, C.; Hervieu, M.; Raveau, B. *Solid State Commun.* **2001**, *117*, 377.
(10) Taniguchi, T.; Mizusaki, S.; Okada, N.; Nagata, Y.; Lai, S. H.; Lan, M. D.; Hiraoka, N.; Itou, M.; Sakurai, Y.; Ozawa, T. C.; Noro, Y.; Samata, H. *Phys. Rev. B* **2008**, *77*, 014406.

Published on Web 08/17/2009

absorption near edge structure (XANES) spectroscopy, which is a powerful element specific experimental probe for the investigation of the electronic structures of complex oxides. Previously XANES has shown the presence of mixed valence $Ru^{4+/5+}$ in the structurally related system $La_{1+x}Ca_{1-x}RuCoO_6$, although in these Co-containing oxides the Co is present only as Co^{2+}.[11] Mossbauer studies of $CaRu_{0.85}Fe_{0.15}O_3$ show the Fe is present as Fe^{3+}, requiring partial oxidation of the Ru^{4+} to Ru^{5+} to maintain charge balance.[12] The coexistence of mixed valence redox pairs involving both $Mn^{3+/4+}$ and $Ru^{4+/5+}$ has also been observed in XANES studies of the related $SrRu_{1-x}Mn_xO_3$ system.[13,14]

Just as there is a dearth of experimental studies providing direct experimental evidence for $Mn^{3+/4+}$ and $Ru^{4+/5+}$redox pairs, there are few high resolution structural studies available in the $CaRu_{1-x}Mn_xO_3$ system. Almost without exception, structural investigations have been limited to polycrystalline samples using nonmonochromatic Cu radiation, an approach that rarely yields accurate and precise bond distances or angles for low symmetry oxides containing heavy metals. The notable exceptions are the oxides $CaRu_{0.4}Mn_{0.6}O_3$ and $CaRu_{0.5}Mn_{0.5}O_3$ that have been structurally characterized using powder neutron diffraction methods. In the former case, Yoshii et al.[15] reported that partial ordering of the Ru and Mn cations was present in $CaRu_{0.4}Mn_{0.6}O_3$ lowering the symmetry to monoclinic, although Sharmes et al.[16,17] described the structure of $CaRu_{1-x}Mn_xO_3$ ($x \geq 0.60$) to be orthorhombic in *Pbnm*—that is without any cation ordering. Lufaso and co-workers[18] concluded that the Ru and Mn cations were disordered in a single crystallographic site in $CaRu_{0.5}Mn_{0.5}O_3$, and the appropriate space group was *Pbnm*. Neutron powder diffraction has also been used to study the magnetic structures of some Mn rich members in $CaRu_{1-x}Mn_xO_3$ ($x \geq 0.60$) although no structural parameters were reported in their work.[16]

In order to understand the unique physical properties of the Ru/Mn oxides, it is important to ascertain the relationships between the electronic, magnetic, and crystal structures. In this report, we describe XANES, synchrotron X-ray and neutron powder diffraction studies of the series $CaRu_{1-x}Mn_xO_3$. We provide direct experimental evidence for the presence of both $Mn^{3+/4+}$ and $Ru^{4+/5+}$ redox pairs in this series and demonstrate that complex phase segregation is also present. The Mn and Ru oxidations states were also derived from least-squares fits of the Mn K- and Ru L_3-edge XANES spectra.

Experimental Section

Polycrystalline samples of 11 members of the series $CaRu_{1-x}Mn_xO_3$ were prepared by conventional solid state reaction using high purity $CaCO_3$ (99.95%), MnO_2 (99.999%), and Ru (99.99%). The appropriate stoichiometric amounts of the starting materials, sufficient to prepare ca. 1 g of each sample, were mixed in an agate mortar, and the mixture was calcined at 700 °C for 20 h. The samples were then reground and fired at 1100 °C for 20 h and 1150 °C for 7 days. The samples were periodically reground during the reaction which was continued, until the diffraction patterns no longer changed and the samples appeared homogeneous.

X-ray absorption measurements were performed at the National Synchrotron Radiation Research Center (NSRRC) in Hsinchu, Taiwain.[19] Ru L-edge and Mn K-edge spectra were recorded in fluorescence mode on beamline BL-16A1 using a Lytle detector from powder samples dispersed on Kapton tape. Low temperature measurements were performed using a ARS DE-202G Closed Cycle Cryostat. For these measurements, the powder samples were mixed with Apiezon Grease (Type N) and dispersed onto a copper plate in contact with the cryostat cold head. Energy steps as small as 0.2 eV were employed near the absorption edges with a counting time of 2 s per step. The spectra were normalized to the incident photon current. The energy scale of the Ru $L_{3,2}$- and Mn K-edge spectra was calibrated using the L_2-edge of a Mo foil and K-edge of a Mn foil respectively. Sr_2RuYO_6 and La_2MnRhO_6 were used as the Ru^{5+} and Mn^{3+} standards, and the end members of $CaRuO_3$ and $CaMnO_3$ as standards for Ru^{4+} and Mn^{4+}. Data analysis was carried out using a suite of programs within the software package EXAFSPAK.[20] First the BACKSUB program was used for background subtraction and normalization, followed by principal component analysis (PCA), target transformation (TARGET), and least-squares refinement (DATFIT).

The synchrotron X-ray diffraction data were collected using the MYTHEN microstrip detector on the powder diffractometer at BL-10 of the Australian Synchrotron in Melbourne, Australia.[21] The samples were housed in 0.3 mm diameter glass capillaries that were rotated during the measurements. Data were recorded at room temperature in the angular range $5° < 2\theta < 65°$, using X-rays of wavelength 0.82691 (1) Å as estimated using NIST LaB_6. Neutron diffraction data were collected for $CaRu_{0.5}Mn_{0.5}O_3$ at room temperature in the angular range $10° < 2\theta < 160°$ with neutrons of wavelength 1.538(1) Å using the powder diffractometer Echidna at the Australian Nuclear Science and Technology Organisation's OPAL facility. The structures were refined using the program RIETICA.[22] The higher than typical χ^2 values for the refinement of $CaRuO_3$ reflect the unusual broadening of the peaks, observed in this data, which was relatively poorly modeled by the pseudo-Voigt peak shape.

(11) Bos, J. W. G.; Attfield, J. P.; Chan, T. S.; Liu, R. S.; Jang, L. Y. *Phys. Rev. B* **2005**, *72*, 014101.
(12) Mizusaki, S.; Taniguchi, T.; Okada, N.; Nagata, Y.; Hiraoka, N.; Nagao, T.; Itou, M.; Sakurai, Y.; Ozawa, T. C.; Noro, Y. *J. Appl. Phys.* **2006**, *99*, 08F703.
(13) Sahu, R. K.; Hu, Z.; Rao, M. L.; Manoharan, S. S.; Schmidt, T.; Richter, B.; Knupfer, M.; Golden, M.; Fink, J.; Schneider, C. M. *Phys. Rev. B* **2002**, *66*, 144415.
(14) Manoharan, S. S.; Sahu, R. K. *Chem. Commun.* **2002**, 3068.
(15) Yoshii, K.; Nakamura, A.; Mizumaki, M.; Tanida, H.; Kawamura, N.; Abe, H.; Ishii, Y.; Shimojo, Y.; Morii, Y. *J. Magn. Magn. Mater.* **2004**, *272*, E609.
(16) Shames, A. I.; Rozenberg, E.; Martin, C.; Maignan, A.; Raveau, B.; Andre, G.; Gorodetsky, G. *Phys. Rev. B* **2004**, *70*, 134433.
(17) Shames, A. I.; Rozenberg, E.; Martin, C.; Maignan, A.; Raveau, B.; Andre, G.; Gorodetsky, G. *J. Supercond. Novel Magn.* **2007**, *20*, 99.
(18) Lufaso, M. W.; Woodward, P. M.; Goldberger, J. *J. Solid State Chem.* **2004**, *177*, 1651.
(19) Dann, T. E.; Chung, S. C.; Huang, L. J.; Juang, J. M.; Chen, C. I.; Tsang, K. L. *J. Synchrotron Rad.* **1998**, *5*, 664.
(20) George, G. N.; Pickering, I. J. *EAXFSPAK: A Suite of Computer Programs for Analysis of X-ray Absorption Spectra*; Stanford Synchrotron Radiation Laboratory: Menlo Park, CA, 2000.
(21) Wallwork, K. S.; Kennedy, B. J.; Wang, D. *AIP Conf. Proc.* **2007**, *879*, 879.
(22) Hunter, B. A.; Howard, C. J.; In *A Computer Program for Rietveld Analysis of X-Ray and Neutron Powder Diffraction Patterns*; Lucas Heights Research Laboratories: Sydney, 1998; p 1.

Results and Discussion

1. Structure. The X-ray diffraction patterns of all the samples suggested that all members of the $CaRu_{1-x}Mn_xO_3$ series adopt an orthorhombic $GdFeO_3$-type perovskite structure at room temperature with space group *Pbnm*, and initially structures for the 11 compositions in the series were refined in this space group. Refinements of the structures for the two end-member oxides $CaRuO_3$ and $CaMnO_3$ yielded values in excellent agreement with those previously reported (Table 1). In particular, the refined Mn−O bond distances in $CaMnO_3$ were within three combined standard deviations of the values reported using powder neutron diffraction data.[23] Those for $CaRuO_3$ are in good agreement with the values calculated from the atomic coordinates reported by Rajan et al.[24] for $CaRuO_3$ at 150 °C, demonstrating the ability of the high resolution synchrotron diffraction data to yield accurate and precise structures, even in the presence of the heavy Ru cation.

No evidence was found from any of the samples to support the hypothesis of Yoshii et al.[15] that rock saltlike ordering of the Ru and Mn cations, resulting in lowering of the symmetry to monoclinic in $P2_1/n$, occurred for $CaMn_{0.6}Ru_{0.4}O_3$. Critically, no intensity was observed for the 110 reflection near $d = 4.35$ Å ($2\theta = 10.90°$) in the synchrotron diffraction pattern for this oxide. Indeed refinements in this monoclinic space group returned occupancies within one standard deviation of a random distribution of the Ru and Mn over the two crystallographically distinct sites and yielded comparable *R*-factors to the fits in *Pbnm*.

However, the single-phase fits for the samples with $x = 0.2-0.4$ were somewhat poorer than those obtained for the other samples. Careful examination of the patterns suggested the presence of two distinct orthorhombic phases in these samples, and the two-phase model also results in more satisfactory fits for samples with $x = 0.1$, 0.5, and 0.6, suggesting that phase separation occurred for all six oxides with $x = 0.1-0.6$. In refining the two structures, the atomic displacement parameters for each type of atom were constrained to be equal and it was assumed that the instrumental profile parameters for the two phases were identical. No constraints were placed on either the lattice parameters or atomic coordinates of the two phases. This strategy resulted in acceptable fits for all compositions, although the estimated errors for the second phase were larger than optimal (See Table 2). We hasten to add that the diffraction patterns for the samples recorded using nonmonchromated Cu radiation did not reveal any evidence for the coexistence of these phases, and in all cases adequate fits were obtained to such data using a single phase model. This explains why only one phase was detected by Tanigushi et al.,[10] who used a nonmonchromated laboratory X-ray source in their

Table 1. Rietveld Refinement Results for $CaRu_{1-x}Mn_xO_3$ from Synchrotron X-ray Diffraction Data Obtained at RoomTemperature[a]

x	0	0.1	0.2	0.3	0.4	0.5	0.6	0.7	0.8	0.9	1.0
a (Å)	5.36417(10)	5.37261(12)	5.35978(11)	5.35191(7)	5.34625(6)	5.33909(6)	5.32854(5)	5.31745(4)	5.30350(2)	5.28790(1)	5.26750(1)
b (Å)	5.52380(10)	5.48935(10)	5.47933(9)	5.46502(8)	5.44380(7)	5.41953(7)	5.39440(5)	5.36591(4)	5.33952(2)	5.31229(1)	5.28276(1)
c (Å)	7.66617(14)	7.64407(23)	7.62952(21)	7.61418(9)	7.59770(8)	7.57844(8)	7.55824(6)	7.53844(5)	7.51485(3)	7.48856(2)	7.45752(1)
Ca *x*	0.0073(6)	0.0085(17)	0.0055(10)	0.0040(7)	0.0028(6)	0.0045(5)	0.0050(4)	0.0055(4)	0.0063(3)	0.0062(2)	0.0056(1)
Ca *y*	0.5519(2)	0.5462(5)	0.5474(2)	0.5497(2)	0.5476(1)	0.5429(1)	0.5396(1)	0.5368(1)	0.5364(1)	0.5346(1)	0.5323(1)
Ca B_{iso}	1.63(3)	0.88(1)	0.98(1)	0.79(2)	0.84(1)	0.92(1)	0.97(1)	0.97(1)	0.83(1)	0.72(1)	0.38(1)
Ru/Mn B_{iso}	1.21(1)	0.61(1)	0.63(1)	0.59(1)	0.59(1)	0.59(1)	0.49(1)	0.50(1)	0.41(1)	0.30(1)	0.15(1)
O1 *x*	−0.0824(7)	−0.1075(20)	−0.0895(11)	−0.0898(8)	−0.0898(7)	−0.0888(7)	−0.0790(5)	−0.0837(5)	−0.0744(4)	−0.0679(3)	−0.0690(3)
O1 *y*	−0.0211(9)	−0.0120(20)	−0.0201(9)	−0.0229(7)	−0.0160(6)	−0.0135(6)	−0.0147(4)	−0.0166(5)	−0.0146(3)	−0.0115(2)	−0.0108(2)
O1 B_{iso}	1.96(1)	1.17(5)	1.33(6)	1.60(9)	1.02(7)	0.55(7)	0.40(5)	1.21(6)	1.53(5)	1.50(3)	0.37(3)
O2 *x*	0.2108(6)	0.2114(20)	0.2125(9)	0.2072(5)	0.2035(5)	0.2057(5)	0.2061(4)	0.2074(4)	0.2090(3)	0.2120(2)	0.2135(2)
O2 *y*	0.2907(6)	0.2929(12)	0.2882(6)	0.2853(5)	0.2856(5)	0.2881(4)	0.2896(3)	0.2892(3)	0.2867(2)	0.2858(2)	0.2878(2)
O2 *z*	0.0543(4)	0.0475(13)	0.0438(5)	0.0452(4)	0.0427(3)	0.0386(3)	0.0401(3)	0.0331(3)	0.0346(2)	0.0353(2)	0.0348(2)
O2 B_{iso}	1.70(8)	2.57(4)	1.70(6)	0.88(6)	1.10(6)	1.08(6)	1.49(5)	1.65(5)	1.18(3)	0.88(2)	0.30(2)
R_p	5.29	2.48	2.50	2.72	5.44	2.56	2.62	2.63	2.34	2.78	3.14
R_{wp}	6.76	3.54	3.54	3.94	4.20	3.71	3.77	3.89	3.51	4.02	4.80
χ^2	47.05	15.56	13.96	15.71	18.01	13.47	15.88	14.31	11.99	15.29	18.58
wt %	100	12.9(5)	74.8(6)	79.9(2)	87.8(2)	91.8(3)	93.8(2)	100	100	100	100
M−O1	1.971(1)	2.0003(9)	1.970(2)	1.967(3)	1.961(8)	1.954(11)	1.938(12)	1.938(6)	1.9213(4)	1.9072(3)	1.9004(3)
M−O2	2.008(4)	1.996(2)	1.975(5)	1.944(7)	1.925(10)	1.932(16)	1.934(18)	1.920(2)	1.908(15)	1.906(11)	1.909(10)
M−O2	1.979(4)	1.966(3)	1.959(5)	1.988(7)	1.995(10)	1.967(18)	1.958(18)	1.940(2)	1.936(15)	1.919(11)	1.898(10)
M−O (avg)	1.986	1.988	1.968	1.966	1.960	1.951	1.943	1.933	1.922	1.911	1.902

[a] All refinements were carried out in orthorhombic symmetry (space group *Pbnm*) with Ca on a 4*c* (*x*, *y*, 1/4) site, Mn/Ru on a 4*b* (0, 0, 0) site, O1 on a 4*c* (*x*, *y*, 1/4) site, and O2 on an 8*d* (*x*, *y*, *z*) site. Where two phases were observed, the weight percent of the tabulated phase derived from the Rietveld analysis is given.

(23) Bozin, E. S.; Sartbaeva, A.; Zheng, H.; Wells, S. A.; Mitchell, J. F.; Proffen, T.; Thorpe, M. F.; Billinge, S. J. L. *J. Phys. Chem. Solids* **2008**, *69*, 2146.
(24) Ranjan, R.; Senyshyn, A.; Vashook, V.; Niewa, R.; Boysen, H.; Frey, F. *Appl. Phys. Lett.* **2007**, *90*, 251913.

Table 2. Lattice parameters for the second phase in the series $CaRu_{1-x}Mn_xO_3$ as determined from synchrotron X-ray diffraction data obtained at room temperature

x	0.1	0.2	0.3	0.4	0.5	0.6
a (Å)	5.35996(4)	5.35862(11)	5.3580(2)	5.3520(2)	5.3416(3)	5.3303(4)
b (Å)	5.51702(5)	5.51163(10)	5.5130(2)	5.5044(3)	5.4873(3)	5.4654(4)
c (Å)	7.65439(5)	7.6459(3)	7.6492(2)	7.6339(3)	7.6058(4)	7.5688(5)

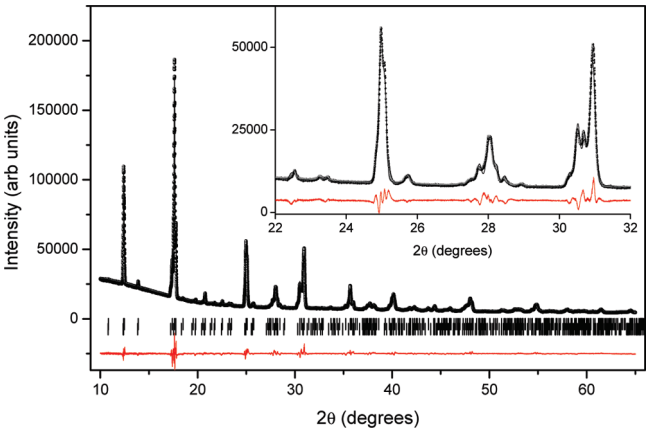

Figure 1. Rietveld refinement profiles for $CaRu_{0.7}Mn_{0.3}O_3$. The inset illustrates the detail of the fit and shows the broadening due to the presence of the two phases. The final R-factors were R_p 2.72 and R_{wp} 3.94%. The values for the fit to a single phase orthorhombic model were R_p 3.77 and R_{wp} 5.79%.

structural study of $CaRu_{1-x}Mn_xO_3$. That we find evidence for two orthorhombic *Pbnm* phases is not inconsistent with the electron diffraction studies of Maignan et al.[9] Electron diffraction measurements are not sufficiently accurate to distinguish two similar cells in the same space group. Our present results are a powerful illustration of the benefits of using high resolution diffraction data in the study of complex oxides. An example of the diffraction profiles is presented in Figure 1 for $CaRu_{0.7}Mn_{0.3}O_3$.

To exclude the possibility that the observed phase segregation was a consequence of the synthesis conditions we have annealed portions of the sample of $CaRu_{0.5}Mn_{0.5}O_3$ at 900 °C for 24 h under flowing O_2 or Ar. Structural refinements of the synchrotron X-ray diffraction patterns revealed that annealing under O_2 or Ar did not alter the phase composition of the air sintered sample (Figure 2). While the relative abundance of the two phases did not change, annealing did alter the lattice parameters of the second phase, as is evident from Figure 2.

The orthorhombic *Pbnm* model has three independent M−O bond distances. For every composition, the three bond distances refine to approximately the same value; Table 1. The average M−O distance is observed to systematically decrease with increasing Mn content. The accuracy of the refinements is evident in the case of $CaRu_{0.5}Mn_{0.5}O_3$, where the three M−O distances were 1.954(11), 1.932(16), and 1.967(18) Å (average 1.951 Å) in good agreement with those obtained in the present work using neutron diffraction data 1.951(4), 1.934(2), and 1.957(4) Å (average 1.947 Å). As a consequence of the lower peak-width resolution of the neutron diffraction

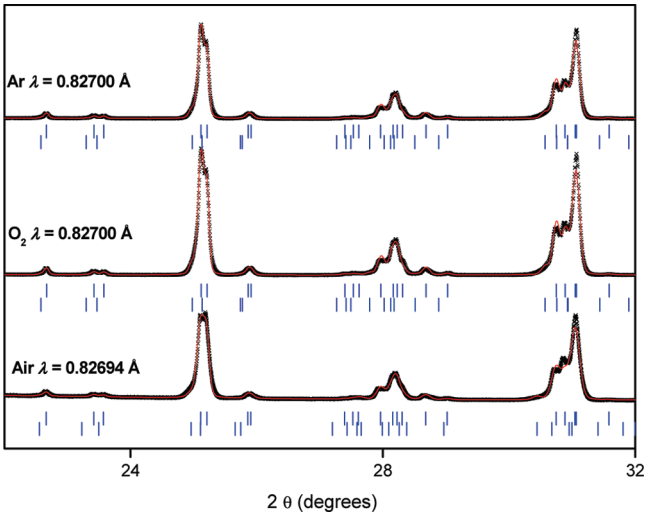

Figure 2. Portions of the Rietveld refinement profiles for $CaRu_{0.5}Mn_{0.5}O_3$, annealed under different conditions, illustrating the persistence of the phase separation.

data, it was not possible to refine the structure for the two orthorhombic phases, rather the neutron data were fitted using a single phase orthorhombic model. [The refined lattice parameters from the neutron diffraction were the following: $a = 5.3412(3)$, $b = 5.4212(3)$, and $c = 7.5859(5)$ Å. The refined atomic parameters (x, y, z) were the following: Ca 0.0069(9), 0.5424(6), 0.25; Ru/Mn 0, 0, 0; O(1) −0.0771(5), −0.0177(5), 0.25; O(2) 0.2035(4), 0.2938(3), 0.0403(3).] It is evident from Figure 3 that the a- and c-parameters for the two phases are approximately equal, with the b-parameter for the second phase being larger. The diffraction data, while not definitive, suggest the assumption of stoichiometric oxygen content is valid. There was no indication from the neutron diffraction data for any anion vacancies. Likewise, the displacement parameters for the two independent anions estimated from the synchrotron diffraction data, Table 1, are unexceptional and suggest the absence of appreciable oxygen vacancies.

The expansion in the b-parameter evident in the second phase results in this having a larger cell volume (Figure 4). In neither phase does the cell volume obey Vegard's law. Figure 4 also shows that the cell volume of "phase 1" agrees very well with that reported by Taniguchi et al.[10] As previously postulated by these authors,[10] and demonstrated by the XANES results presented in the next section, the nonlinear evolution of the cell volume with increasing Mn content is a consequence of the simultaneous introduction of the Mn^{3+} (0.645 Å), Mn^{4+} (0.53 Å), and Ru^{5+} (0.565 Å) cations onto the Ru^{4+} sites (0.62 Å).[25] Given the presence of the Jahn−Teller active Mn^{3+} ion in these oxides, it is possible that the larger cell volume is a consequence of this phase exhibiting orbital ordering, similar to that observed in doped perovskite manganites $Ln_{0.7}A_{0.3}MnO_3$ (where Ln is a trivalent lanthanide and A = Ca, Sr, Ba).[26] As is

(25) Shannon, R. D. *Acta Crystallogr., Sect. A* **1976**, *32*, 751.
(26) Chapman, J. P.; Attfield, J. P.; Rodriguez-Martinez, L. M.; Lezama, L.; Rojo, T. *Dalton Trans.* **2004**, 3026.

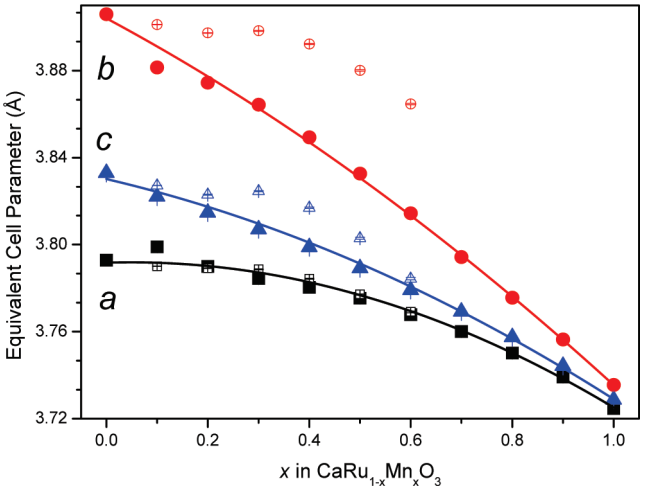

Figure 3. Evolution of the reduced lattice parameters for the two orthorhombic phases (*Pbnm*) in the series $CaRu_{1-x}Mn_xO_3$. The two phases are distinguished by the use of open and closed symbols. The solid lines serve as a guide to the eye for the variation in the major phase.

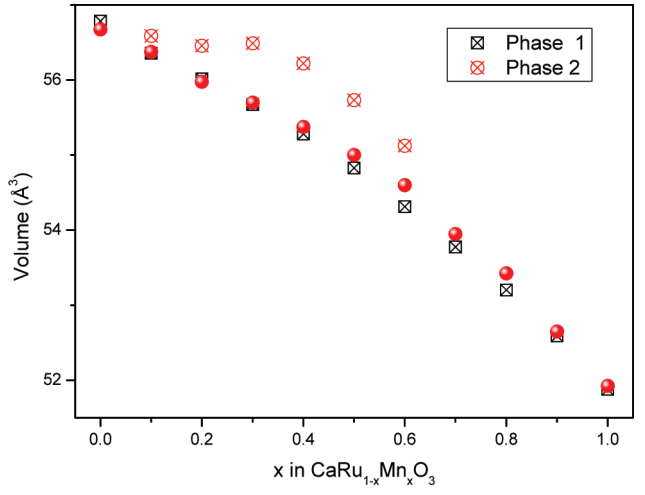

Figure 4. Evolution of the equivalent primitive cell volumes for the two orthorhombic phases (*Pbnm*) in the series $CaRu_{1-x}Mn_xO_3$. The results from the previous study by Taniguchi et al.[10] are indicated by the closed symbols.

well-documented for $LaMnO_3$, orbital ordering increases the cell volume above that otherwise expected.[27] Alternatively, it may be possible that the increased volume for the second phase reflects a greater amount of Mn^{3+} character. Considering the sizes of the four cations that occupy the octahedral site in these perovskites, it is apparent that the presence of Mn^{3+} will dominate the expansion of the lattice because of the larger difference between the relative size of the Mn^{3+} (0.645 Å) and Mn^{4+} (0.53 Å) than that of the Ru^{4+} (0.62 Å) and Ru^{5+} (0.565 Å) cations, ~18 vs 9%. However, the samples appeared to be chemically homogeneous within the accuracy of analytical electron microscopy, and there is no evidence for segregation into two phases having significantly different chemical compositions (although electron microscopy is not able to distinguish between Mn^{3+} and Mn^{4+} or Ru^{4+} and Ru^{5+}).

The coexistence of crystallographically distinct phases in chemically homogeneous systems has been reported for several perovskite systems, most importantly various manganites[26] but increasingly in other systems such as $SmVO_3$[28] and $SrCrO_3$.[29] It was initially postulated that phase separation in the manganite perovskites was a consequence of the strains associated with A-site cation disorder,[30] although the discovery of phase separation in pure $SmVO_3$ and $SrCrO_3$ illustrates that such disorder is not a requirement for this to occur. Mixed valence Mn^{3+}/Mn^{4+} manganites are known to exhibit charge carrier segregation at a submicroscope level, a phenomena that can be enhanced by doping on the Mn sites.[31] In the present case, we postulate that the phase separation reflects the coexistence of two electronically distinct (i.e., orbitally ordered and disordered) phases, as reported by Chapman et al.[26]

In their magnetic studies of $CaRu_{1-x}Mn_xO_3$, Sharmes et al.[16] noted the existence of two *Pbnm* phases, albeit at higher Mn contents than found here. These workers concluded that phase separation between the ferromagnetic and antiferromagnetic phases occurred. These workers did not, however, identify the microscopic nature of the separation. In another study of manganite perovskites, Radaelli et al.[32] observed phase separation in $Pr_{0.7}Ca_{0.3}MnO_3$ using high-resolution neutron diffraction.

2. XANES. A major aim of this work was to obtain direct experimental evidence for the formation of $Mn^{3+/4+}-Ru^{4+/5+}$ redox pairs and to determine the average Mn and Ru oxidation states in these materials using XANES. The Ru L_3-edge XANES spectra of the $CaRu_{1-x}Mn_xO_3$ perovskites are shown in Figure 5. Previous studies have demonstrated that the Ru L_3-edge of Ru^{5+} oxides such as $Sr_4Ru_2O_9$[33] and Sr_2RuGdO_6[34] are characterized by a well-resolved doublet corresponding to the transition from Ru 2p to 4d orbitals, where separate transitions to the t_{2g} and e_g orbitals are observed.[33,34] By comparison, the Ru L_3-edge spectra of Ru^{4+} oxides are typically comprised of a less well resolved doublet, due to less separation of the two peaks and lower intensity in the t_{2g}-related peak.[33,34] At the same time, the Ru L_3-edge appears at higher energy (by ~1.5 eV) in the Ru^{5+} oxides than it does in the Ru^{4+} oxides.[33,34] The position and appearance of the Ru L_3-edge spectra obtained for $CaRu_{0.1}Mn_{0.9}O_3$, illustrated in Figure 5, is indicative of the presence of Ru^{5+} as postulated by previous researchers.[10] Increasing the Ru content leads to a progressive loss of

(27) Chatterji, T.; Fauth, F.; Ouladdiaf, B.; Mandal, P.; Ghosh, B. *Phys. Rev. B* **2003**, *68*, 052406.
(28) Sage, M. H.; Blake, G. R.; Nieuwenhuys, G. J.; Palstra, T. T. M. *Phys. Rev. Lett.* **2006**, *96*, 036401.
(29) Ortega-San-Martin, L.; Williams, A. J.; Rodgers, J.; Attfield, J. P.; Heymann, G.; Huppertz, H. *Phys. Rev. Lett.* **2007**, *99*, 255701.
(30) Rao, G. H.; Barner, K.; Brown, I. D. *J. Phys.: Condens. Matter* **1998**, *10*, L757.
(31) Knizek, K.; Hejtmanek, J.; Jirak, Z.; Martin, C.; Hervieu, M.; Raveau, B.; Andre, G.; Bouree, F. *Chem. Mater.* **2004**, *16*, 1104.
(32) Radaelli, P. G.; Ibberson, R. M.; Argyriou, D. N.; Casalta, H.; Andersen, K. H.; Cheong, S. W.; Mitchell, J. F. *Phys. Rev. B* **2001**, *63*, 172419.
(33) Hu, Z.; von Lips, H.; Golden, M. S.; Fink, J.; Kaindl, G.; de Groot, F. M. F.; Ebbinghaus, S.; Reller, A. *Phys. Rev. B* **2000**, *61*, 5262.
(34) Liu, R. S.; Jang, L. Y.; Hung, H. H.; Tallon, J. L. *Phys. Rev. B* **2001**, *63*, 212507.

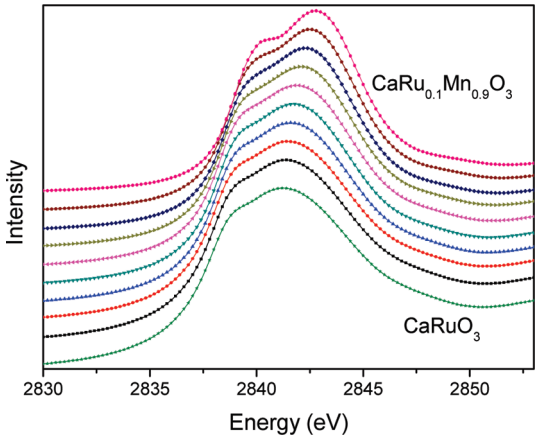

Figure 5. Composition dependence of the Ru L_3-edge XANES spectra for the series $CaRu_{1-x}Mn_xO_3$. The spectra are vertically offset for clarity.

separation of the two peaks and a shift to lower energy, demonstrating a reduction of the formal oxidation state. Within the resolution of the spectral data, this transition is gradual rather than abrupt. The Ru L_2-spectra were also examined, and while not illustrated here, showed similar trends.

The Ru L_3-edge XANES spectra were also used to derive the Ru oxidation state in $CaRu_{1-x}Mn_xO_3$. Principal component analysis (PCA) of the $CaRu_{1-x}Mn_xO_3$ series was performed over the energy range of 2780−2950 eV (corresponding to the Ru L_3-edge), using the PCA program belonging to the EXAFSPAK suite.[20] This analysis suggested that there were only two significant components in the spectra of $CaRu_{1-x}Mn_xO_3$ (x = 0−0.9). Target transformation analysis (TARGET)[20] further demonstrated that the two end members in the series ($CaRuO_3$ and $CaRu_{0.1}Mn_{0.9}O_3$) were excellent choices as those two components. The Ru L_3-edge XANES spectra of the intermediate samples (x = 0.1−0.8) were then fitted with a linear combination of the two end members over the energy range of 2800−2900 eV, using a least-squares refinement program (DATFIT).[20] In order to derive the Ru oxidation state in the intermediate samples, it was necessary to first determine that in $CaRu_{0.1}Mn_{0.9}O_3$. This was achieved by a least-squares fit of the $CaRu_{0.1}Mn_{0.9}O_3$ spectrum to those of the Ru^{4+} and Ru^{5+} standards ($CaRuO_3$ and Sr_2RuYO_6), giving rise to a Ru oxidation state of 4.8 for $CaRu_{0.1}Mn_{0.9}O_3$. We note that although the Ru^{5+} standard, Sr_2RuYO_6, has a different structure to the systems being studied here, both contain RuO_6 octahedra. The variation of the Ru oxidation state with Mn content (x) in $CaRu_{1-x}Mn_xO_3$ is shown in Figure 6, increasing from 4 (x = 0) to 4.8 (x = 0.9). Our results agree qualitatively with those proposed by Taniguchi et al.,[10] who derived the percentages of Ru^{4+}, Ru^{5+}, Mn^{3+}, and Mn^{4+} based on unit cell volumes (and Shannon's effective ionic radii[25]).

Ru $L_{3,2}$-edge XANES spectra were also collected for $CaRu_{0.1}Mn_{0.9}O_3$ at five temperatures between 8 and 300 K. Examination of the spectra did not reveal any appreciable changes upon cooling, suggesting that the electronic state of the Ru remains unaltered. We then

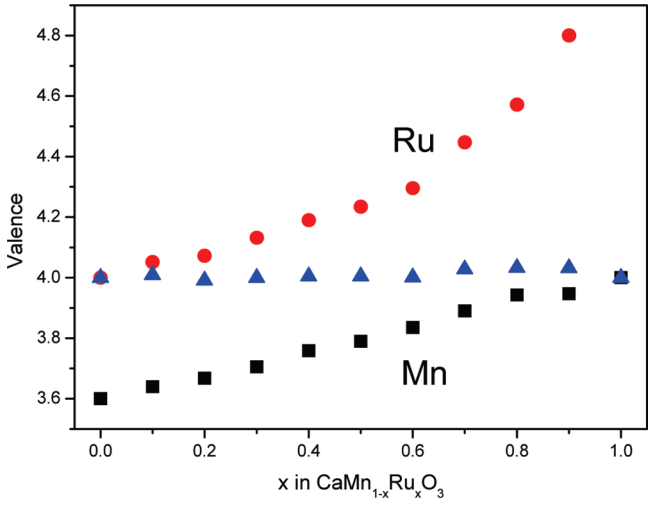

Figure 6. Variation of the Ru (circles) and Mn (squares) oxidation states with x in $CaRu_{1-x}Mn_xO_3$, as well as the sum (triangles) of the B-site cation oxidation state.

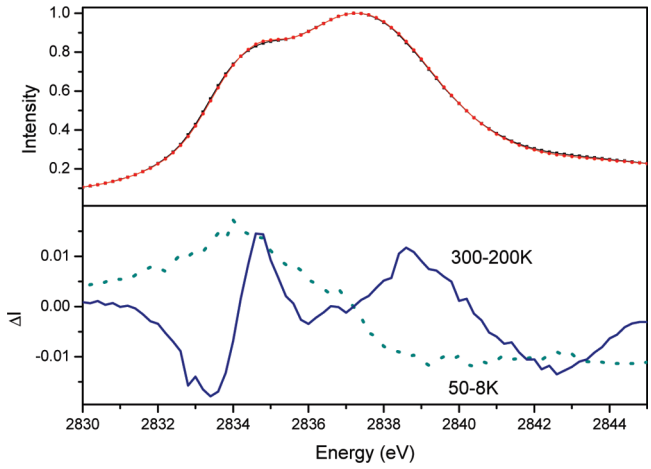

Figure 7. XANES spectra at the Ru L_3-edge for $CaRu_{0.1}Mn_{0.9}O_3$. The upper panel shows the spectra at 8 and 300 K. The lower panel shows the difference between the spectra recorded at 300 and 200 K (solid line) and between those measured at 50 and 8 K (dotted line).

examined difference spectra obtained by subtracting spectra recorded at different temperatures from each other. The difference spectra between the Ru L_3-edge XANES spectra recorded at 300 and 200 K and between those recorded at 8 and 50 K are shown in Figure 7. The former reveals a derivative like feature corresponding to a shift in the absorption edge. This feature is only apparent upon cooling from 300 to 200 K and is not observed in any subsequent difference profiles (e.g., upon cooling from 200 to 100 K). It is possible that the observed subtle changes reflect changes in the magnetic properties of the sample. A similar observation has been made for the mixed valent manganese oxide $La_{0.67}Ca_{0.33}MnO_3$.[35]

Mn K-edge XANES spectra were also obtained from $CaRu_{1-x}Mn_xO_3$ at room temperature, and two of these are shown in Figure 8. The most intense feature at the edge is related to the dipole allowed 1s → 4p transition. The

(35) Subias, G.; Garcia, J.; Proietti, M. G.; Blasco, J. *Phys. Rev. B* **1997**, *56*, 8183.

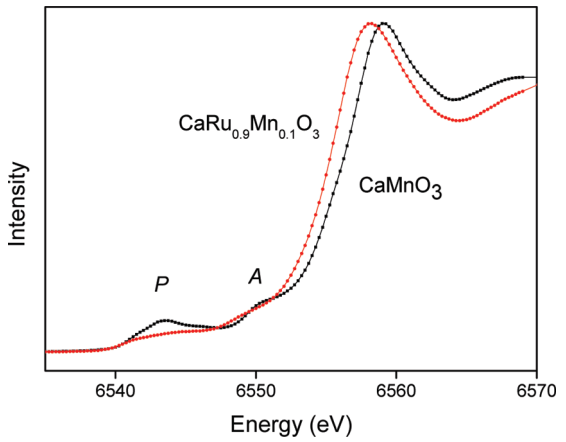

Figure 8. Mn K-edge XANES spectra of $CaMnO_3$ and $CaRu_{0.9}Mn_{0.1}O_3$.

presence of a systematic shift in the K-edge absorption position has been correlated with valence state changes of Mn atoms in manganites,[35] although Ignatov et al.[36] have indicated that changes in the local distortion of the Mn-O_6 octahedra can also lead to a spectral intensity redistribution resulting in an apparent edge shift even in the absence of a valence state change. Our structural refinements, while yielding average structures, do not provide any evidence for a significant change in the average Mn environment and it is likely that the observed edge shift reflects a change in Mn valency. Earlier workers (see, for example, ref 35) have estimated the energy of the K-edge either from the first inflection point or from the edge crest. In either case, accurately determining the energy can be difficult due to local distortions and/or multiple scattering features. Nevertheless as is evident from Figure 8 there is a shift to lower energies as the Ru content is increased, indicative of increasing Mn^{3+} character in the oxides. This shift is opposite to that seen for the Ru L-edge spectra demonstrating electron transfer between Ru and Mn.

In addition to the diagnostic edge shift the spectra are characterized by two features, labeled P and A in Figure 8. The pre-edge feature P is around 15−20 eV below the K-edge, that is, near $E \sim 6542$ eV. This feature is attributed to transitions from the Mn 1s core electrons into the hybridized 3d/4p orbitals (dipole allowed) and the unoccupied 3d states (quadrupole allowed). It has been shown that increased intensity of this pre-edge feature is associated with increased Mn d-hole count, i.e., higher valence state.[37] The weak near-edge feature A results from the dipole transition of the Mn 1s electrons into the lower energy 4p states (due to the solid state splitting of the 4p levels). This feature is also more prominent in Mn^{4+} compounds, e.g. $CaMnO_3$.[37] Comparing the XANES spectrum of $CaRu_{0.9}Mn_{0.1}O_3$ with that of $CaMnO_3$ (Figure 8), the shift toward lower energy of the main Mn K-edge position, together with much lower spectral weight of the pre-edge (P) and near-edge (A) features, clearly illustrates that there is Mn^{3+} in $CaRu_{0.9}Mn_{0.1}O_3$. The ferromagnetism observed in this system is consistent with a double exchange mechanism involving Mn^{3+} and Mn^{4+} ions.[38]

Similar to the Ru L_3-edge spectra, quantitative analysis was also carried out for the Mn K-edge XANES spectra of $CaRu_{1-x}Mn_xO_3$ using a suite of programs within the EXAFSPAK software package.[20] The Mn oxidation state in $CaRu_{0.9}Mn_{0.1}O_3$ was derived as 3.6 based on the least-squares fit to the spectra of the Mn^{4+} standard ($CaMnO_3$) and Mn^{3+} standard (La_2MnRhO_6). The Mn K-edge XANES spectra of the intermediate samples ($x = 0.2 - 0.9$) were fitted to a linear combination of the two end members ($CaMnO_3$ and $CaRu_{0.9}Mn_{0.1}O_3$) over the energy range of 6500−6670 eV. The Mn oxidation state in $CaRu_{1-x}Mn_xO_3$, as derived from the quantitative analysis of the XANES spectra, is plotted in Figure 6, increasing from 3.6 ($x = 0.1$) to 4 ($x = 1$). At high Mn content ($x \geq 0.7$), the Mn valence is predominantly 4, which is consistent with the observation that phase separation only occurred in samples with lower Mn content ($0.1 \leq x \leq 0.6$), because the orbitally ordered phase depends on the presence of the Jahn−Teller active Mn^{3+} cations. Also shown in Figure 6 is the sum of the B-site cation oxidation state, i.e., $(1 - x)Ru^{m+} + xMn^{n+}$. The fact that the B-site cation valence adds up to 4.0 (ranging from 3.99 to 4.03) supports our conclusion that there are no oxygen vacancies in these samples.

Conclusion

A thorough study of 11 members of the series $CaRu_{1-x}Mn_xO_3$, using Mn K-edge and Ru L-edge XANES spectroscopy and high resolution synchrotron X-ray powder diffraction, is reported. The complex distribution of $Mn^{3+/4+}$−$Ru^{4+/5+}$ redox pairs in this system is quantified for the first time directly from experimental (XANES) results. The nominal oxidation states of Ru and Mn were found to increase gradually with the Mn content (x): Ru from 4 ($x = 0$) to 4.8 ($x = 0.9$) and Mn from 3.6 ($x = 0.1$) to 4 ($x = 1$). Our results demonstrate that the coexistence of the mixed valence redox pairs does not result from simply replacing two Ru^{4+} (or Mn^{4+}) with Ru^{5+} and Mn^{3+} (doping Mn into $CaRuO_3$ or Ru into $CaMnO_3$, respectively), as proposed previously. The $Mn^{3+/4+}$−$Ru^{4+/5+}$ redox pairs account for the unusual variation of the lattice parameters and cell volume with chemical composition, as determined from diffraction studies. The formation of redox pairs was accompanied by phase separation in samples with $0.1 \leq x \leq 0.6$.

Acknowledgment. This work has been partially supported by the Australian Research Council. The work performed at the NSRRC was supported by the Australian Synchrotron Research Program under the Major National Research Facilities Program. The synchrotron X-ray diffraction experiments at the Australian Synchrotron were performed with the help of Dr. Kia Wallwork. We thank Dr. Maxim Avdeev for the collection of the neutron diffraction data.

(36) Ignatov, A. Y.; Khalid, S.; Sujoy, R.; Ali, N. *J. Synchrotron Rad.* **2001**, *8*, 898.
(37) Croft, M.; Sills, D.; Greenblatt, M.; Lee, C.; Cheong, S. W.; Ramanujachary, K. V.; Tran, D. *Phys. Rev. B* **1997**, *55*, 8726.
(38) Raveau, B.; Maignan, A.; Martin, C.; Hervieu, R. *Mater. Res. Bull.* **2000**, *35*, 1579.